Available online at www.sciencedirect.com
ScienceDirect
International Journal of Thermal Sciences 46 (2007) 519–530
International Journal of Thermal Sciences
www.elsevier.com/locate/ijts

Fundamental data on the gas–liquid two-phase flow in minichannels ☆

Hideo Ide [a,*], Akira Kariyasaki [b], Tohru Fukano [c]

[a] *Department of Mechanical Engineering, Faculty of Eng., Kagoshima University, 1-21-40 Koorimoto, Kagoshima 890-0065, Japan*
[b] *Department of Chemical Engineering, Faculty of Eng., Fukuoka University, 8-19-1 Nanakuma, Johnann-ku, Fukuoka 814-0180, Japan*
[c] *Faculty of Engineering, Kurume Institute of Technology, 2228-66, Kamitumachi, Kurume 830-0052, Japan*

Received 10 September 2005; accepted 23 July 2006

Available online 8 September 2006

Abstract

We report on the results of investigations into the characteristics of an air–water isothermal two-phase flow in minichannels, that is, in capillary tubes with inner diameters of 1 mm, 2.4 mm, and 4.9 mm, also in capillary rectangular channels with an aspect ratio of 1 to 9. The directions of flow were vertical upward, horizontal and vertical downward. Based on the authors 15 years of fundamental research into the gas–liquid two-phase flows in circular tubes and rectangular channels, we summarized the characteristics of the flow phenomena in a minichannel with special attention on the flow patterns, the time varying holdup and the pressure loss. The effects of the tube diameters and aspect ratios of the channels on these flow parameters and the flow patterns were investigated. Also the correlations of the holdup and the frictional pressure drop were proposed.

Keywords: Minichannel; Gas–liquid flow; Flow patterns; Void fraction; Pressure drop; Liquid film; Correlation; Capillary

1. Introduction

As heat exchangers have become smaller the information on the flow mechanism of a gas–liquid two-phase mixture flowing concurrently in a narrow channel is needed to improve the performance of compact heat exchangers. Fundamental information such as flow pattern, void fraction and pressure loss are all important parameters in designing a heat exchanger. Much interesting data on such flow parameters has been clarified in capillary circular tubes [1–6] and in narrow rectangular channels [7–13].

We have investigated into the isothermal air–water two-phase flow in minichannels over a wide range of flow conditions in both phases from a fluid dynamic point of view in order to clarify the fundamental points of one component two-phase flow in a mini tube.

We are now experimenting to clarify the flow phenomena in a microchannel with a smaller passage size than a minichannel. Therefore, it is important that we summarize the flow phenomena in a minichannel at this stage.

In this paper we will introduce the experimental data which has been obtained by using the constant electric current method, for obtaining the time fluctuating holdup: CECM developed by Fukano [14]. We will discuss the characteristic phenomena which are commonly seen in the two-phase flow in a minichannel. The dimension of the circular and the rectangular channel are as follow; The inner diameters of the circular tube used were 1 mm, 2.4 mm, and 4.9 mm. As a reference we used data obtained in a previous experiment to compare larger scale tubes, 9 mm tube and 26 mm for horizontal flow. In the case of the rectangular channel the cross sectional dimension were 1 mm × 1 mm, 2 mm × 1 mm, 5 mm × 1 mm and 9.9 mm × 1.1 mm. The directions of flow were vertical upward, vertical downward and horizontal. We investigated the flow patterns, the void fraction and the frictional pressure drop, that is, the effects of the tube diameters of circular tubes and the aspect ratios of rectangular channels on the two-phase flow phenomena.

For a flat channel of 9.9 mm × 1.1 mm, the effects of the flow orientations, vertical and horizontal flows, were also inves-

☆ A preliminary version of this paper was presented at ICMMO5: Third International Conference on Microchannels and Minichannels, held at University of Toronto, June 13–15, 2005, organized by S.G. Kandlikar and M. Kawaji, CD-ROM Proceedings, ISBN: 0-7918-3758-0, ASME, New York.

* Corresponding author. Tel.: +81 99 285 8270; fax: +81 99 285 8270.
E-mail address: ide@mech.kagoshima-u.ac.jp (H. Ide).

1290-0729/$ – see front matter
doi:10.1016/j.ijthermalsci.2006.07.012

Nomenclature

A	long side length of cross section of rectangular channel	mm, m
B	short side length of cross section of rectangular channel	mm, m
C	constant in Eq. (4)	
C_s	constant in Eq. (3)	
D	pipe inner diameter	mm, m
D_e	equivalent diameter defined by Sadatomi et al. [29], $\equiv 2(A+B)/\pi$	mm, m
D_h	hydraulic equivalent diameter, $\equiv 2AB/(A+B)$	mm, m
g	acceleration of gravity	$m\,s^{-2}$
j	volumetric flux	$m\,s^{-1}$
j_T	total volumetric flux	$m\,s^{-1}$
L_G	mean length of a gas bubble	mm or m
L_C	length along tube axis	mm or m
L_L	mean length of a liquid slug	mm or m
L_s	distance between two electrodes for CECM	mm
ΔP_e	expansion loss	Pa
ΔP_f	frictional pressure drop	Pa
r	Radius of curvature of return bend	m
T_s	aspect ratio of cross section of rectangular channel, $\equiv A/B$	
t_{Bm}	mean base film thickness	mm
t_{Sm}	mean liquid film thickness around bubble	mm
u_R	bubble velocity in a stagnant liquid in a pipe	$m\,s^{-1}$
u_s	bubble velocity	$m\,s^{-1}$

Greek symbols

α	void fraction	
α_B	void ratio just upstream of the tail of the bubble	
β	ratio of the gas to the mixture volume rates	
γ	ratio of the gas to the slug unit length $\equiv L_G/(L_G+L_L)$	
η	holdup	
Φ_L	two phase multiplier for frictional pressure drop	
Φ_{LCH}, Φ_L	estimated by the Chisholm correlation	
λ	friction factor	
μ	dynamic viscosity	Pa s
ν	kinematic viscosity	$m^2\,s^{-1}$
ρ	density	$kg\,m^{-3}$
σ	surface tension of the liquid	$N\,m^{-1}$
τ	time lag	ms or s
χ	Martinelli parameter	

Subscripts

T	two-phase mixture
G	gas phase
L	liquid

tigated. In the horizontal flow, the two ways of setting a channel, the transverse and the longitudinal, were tested and we examined how the differences of transverse and longitudinal settings exerted an influence on flow.

It is noticed that the data discussed here was all obtained for air and water flow and the effects on the properties of both phases should be investigated in the future.

2. Experiment

The dimensions of the test section of the circular channels are summarized in Fig. 1. Those for the rectangular duct are shown in Figs. 2 and 3 with the dimension in Table 1. Air is injected from 3 small holes with 0.3 mm or 0.5 mm diameter which are made at intervals of 120 degree on the circumference of the main tube at the air–water mixer, into the liquid flowing in the straight main tube.

Static pressure and pressure difference were measured by pressure transducers. All the data of holdup, i.e., void fraction were measured by the constant electric current method (CECM). CECM is fundamentally a conductance method. The methods characteristics are a constant current power source is used for supplying electric power and two types of electrodes are flush mounted in series in the test section. One is used for supplying electric power and the other for measuring the information about holdup or film thickness. The main advantages of CECM are as follows:

Pipe I.D. mm	A_s mm	L mm	B_s mm	C mm	F mm	L_s mm
1.0	510	260	930	110	265	16.5
2.4	560	257	1168	110	283	32
4.9	878	260	1057	110	410	55

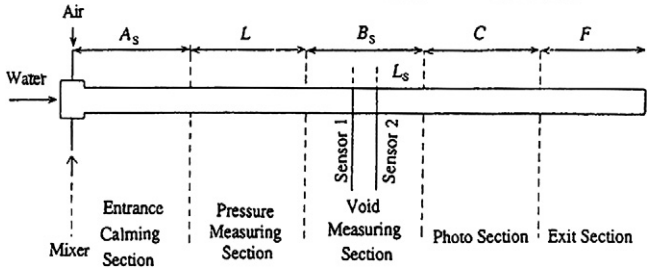

Fig. 1. Dimensions of the test section for the circular channel.

(1) the output from the sensor electrode is independent of the location of the gas phase
(2) the sensitivity for detecting the change in the holdup is higher, in the case of the thinner film thickness, and
(3) the interaction between the electrodes is negligible.

The basic idea, the calibration, and the examples on the application of CECM are described in Ref. [14]. In this paper, two pairs of sensor electrodes are set at two axially different locations to measure the velocities of the bubbles. The outputs of the static pressure, the pressure difference and the holdup are simultaneously sampled at the frequency of 2 KHz or 5 KHz and recorded with a computer. The flow conditions tested in this pa-

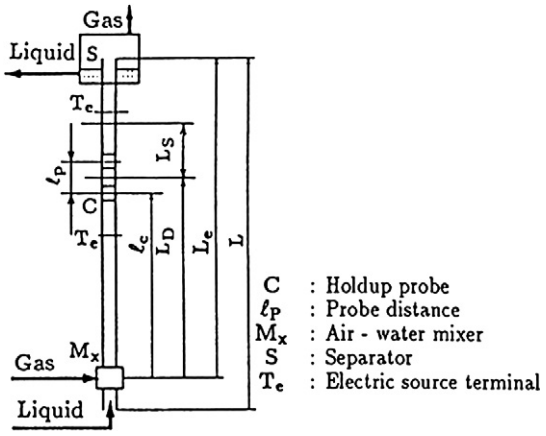

Fig. 2. Experimental setup for rectangular flat channel.

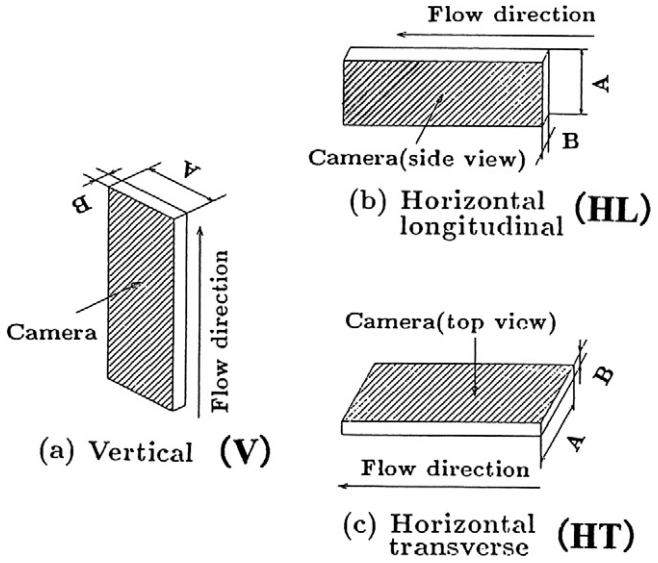

Fig. 3. Orientation of test section.

Table 1
Dimension of test section and probes

$A \times B$	T_s	D_h	D_e	L	L_e	ℓ_c	ℓ_p	t	ℓ_t	L_D	L_s
1.0×1.0	1.0	1.0	1.27	1042	797	315	6.6	0.3	1.0	350	130
2.0×1.0	2.0	1.33	1.91	1254	1089	397	6.6	0.3	1.0	460	130
5.0×1.0	5.0	1.67	3.82	1543	1333	516	6.6	0.3	1.0	580	305
9.9×1.1	9.0	1.98	7.0	1890	1780	751	7.0	0.3	1.3	698	450

t: Thickness of brass plate (for anode and cathode probes) of a wall conductance probe.
ℓ_t:Distance between brass plates in a wall conductance probe.

per are as follows: pressure = 0.15–0.24 MPa, temperature = 291–297 K, superficial gas velocities, $j_G = 0.1$–$30.0\ \mathrm{m\,s^{-1}}$, superficial liquid velocities, $j_L = 0.03$–$2.3\ \mathrm{m\,s^{-1}}$.

3. Experimental results

The distinctive marks on the capillary tube flow are summarized by the following fundamental two points (1) the flow pattern is axisymmetric and (2) the velocity of large gas bubbles relative to a liquid slug is quite low.

3.1. Flow pattern in circular minichannel

Fig. 4 shows the typical vertical upward and downward flows and horizontal flow pattern in 2.4 mm inner diameter (I.D.) tubes, as well as those in 1 mm, 9 mm, and 26 mm I.D. horizontal tubes examining the competing effects of gravitational and surface tension forces.

The characteristics of the flow pattern shown in these photos are summarized as follows:

(a) A separated flow is not really seen in the capillary tubes, which shows that the difference in the flow pattern caused by the difference in the flow direction is small in capillary tubes.
(b) Fig. 4(k) shows a part of a very long air bubble from a horizontal slug flow in the 26 mm I.D. tube, in which we can see that water flows on the bottom side and air on the top side on the slug. The flow pattern in the 9 mm I.D. horizontal pipe with approximately equal flow conditions in the case of Fig. 4(k) is shown in Fig. 4(j). Film thickness at the bottom is much larger than that at the top also in this case. On the other hand, the flow patterns in the 1 mm and 2.4 mm I.D. horizontal pipes are intermittent with comparatively short and axisymmetric bubbles, as shown respectively in Figs. 4(l) and 4(i). We believe these facts signify that the critical tube size at which the surface tension force surpasses the gravitational force is around 5 mm as Bretherton [23] has also described.
(c) As the pipe size decreases the circumferential distribution of the film thickness becomes more uniform, causing axisymmetric flow patterns.
(d) The smaller the pipe size, the thinner the water film around a large air bubble.
(e) Small bubbles in a liquid slug and liquid film are rarely observed in a capillary tube.

3.2. Relation between photographs of the flow and the holdup signals in a rectangular flat minichannel

Fig. 5 shows photographs of the flow in the flat minichannel with a dimension of 9.9 mm × 1.1 mm where superficial gas velocity $j_G = 0.5$–$20\ \mathrm{m\,s^{-1}}$ and superficial liquid velocity $j_L = 0.1\ \mathrm{m\,s^{-1}}$. Fig. 5(a) shows the vertical flow, (b) and (c) show horizontal flow in the longitudinal (HL) transverse (HT) settings, respectively, the flow patterns in each photograph in Fig. 5(a)–(c) can be classified as the slug flow for $j_G = 0.5$ and $1\ \mathrm{m\,s^{-1}}$, the froth flow for $j_G = 3$ and $5\ \mathrm{m\,s^{-1}}$, and the annular flow. In this paper, we refer to this as the annular flow if the surrounding whole wall of the flat channel is covered with liquid film at a higher gas velocity even in a flat channel.

The flow configurations features in the channel with a large aspect ratio are described as follows. In the transition region between the slug and the froth flow, i.e., $j_G \leqslant 1$–$3\ \mathrm{m\,s^{-1}}$ in Fig. 5(a), gas slugs, the noses of which are much flatter than the bullet-like noses observed in a circular tube, rise swinging right and left and the liquid film and large liquid lumps near the wall are entrained in the stream of the gas core.

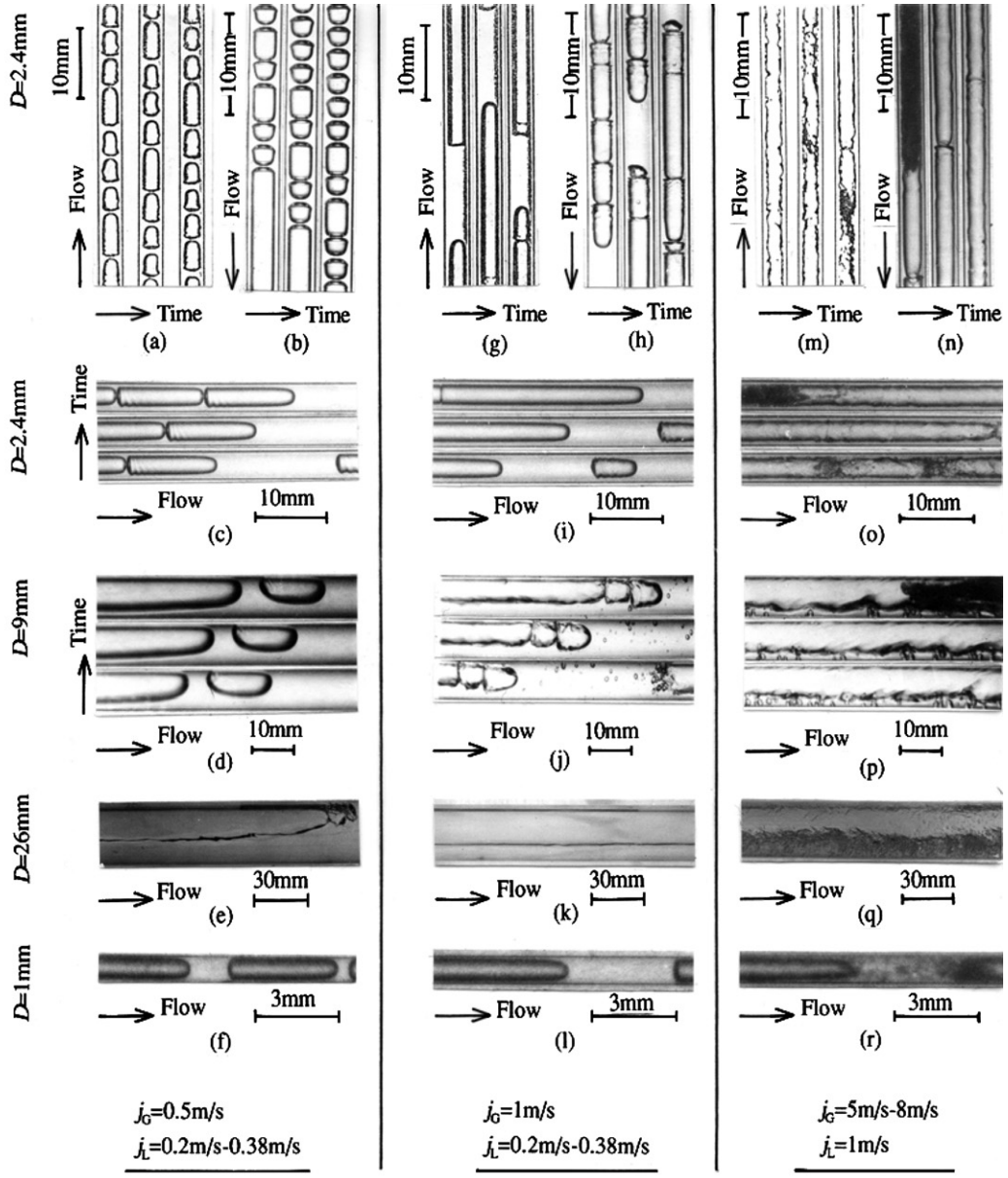

(a), (g), (m) Vertical upward flow, D=2.4 mm
(b), (h), (n) Vertical down ward flow, D=2.4 mm
(c), (i), (o) Horizontal flow, D=2.4 mm
(d), (j), (p) Horizontal flow, D=9 mm
(e), (k), (q) Horizontal flow, D=26 mm
(f), (l), (r) Horizontal flow, D=1 mm

Fig. 4. Typical example of flow pattern.

When $j_G \gtrsim 3\ \mathrm{m\,s^{-1}}$, the flow is considerably different from what we call the Taylor bubble type slug flow and the froth flow in a circular tube. The gas slugs have such complicated shapes that we cannot distinguish noses from tails even in the slug flow. That is, the gas penetrates the large liquid lumps in a complex manner as seen in the figures, which is a feature special to a narrow flat channel.

When $j_G \gtrsim 10\ \mathrm{m\,s^{-1}}$, the gas stream penetrates the liquid slugs, i.e., they are large liquid lumps. Then the flow pattern changes into an annular flow. Disturbance waves and ripple waves can be clearly observed. We observe in Fig. 5(b) that the difference between the liquid film thickness in the top and bottom sides of the channel becomes smaller in cases involving larger values of j_G and that the flow becomes similar to the relatively symmetrical case of vertical flow, (a) V, and the horizontal flow, (c) HT which was photographed from the top of the flat channel.

Fig. 6 shows an example of the time fluctuating output signals from the holdup probes for the 9.9 mm × 1.1 mm channel. (a) of Fig. 6 shows those for the froth flow case and (b) for the annular flow case. (a)–(c) in each figure show respectively the vertical case (V), the horizontal longitudinal case (HL), and the

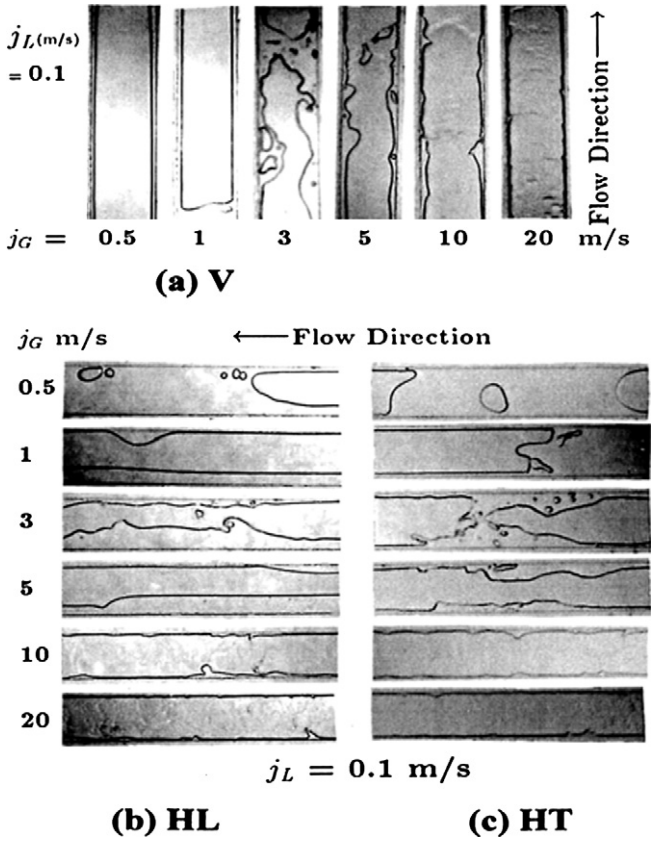

Fig. 5. Examples of photographs of the flow pattern.

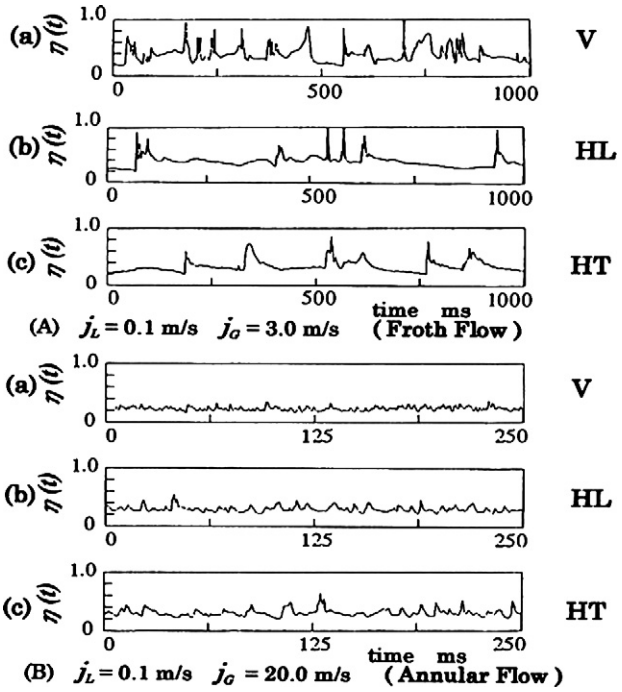

Fig. 6. Examples of the holdup signal (9 mm × 1.1 mm).

horizontal transverse case (HT). The ordinate $\eta(t)$ expresses the holdup. Its value is 1 when the whole area of the cross section is filled with liquid and 0 when it is filled with gas.

Notice that both the passing frequencies of liquid slugs, i.e. $\eta(t) \cong 1$, in Fig. 6(a) and those of very small waves in Fig. 6(b) are high in the vertical case (V) while the passing frequency of the relatively large waves is less in the horizontal flow. We believe that the very small waves make the interfacial shear stress increase as a whole and accordingly the liquid film thickness thins in the vertical flow case.

3.3. Flow pattern map of circular tubes

Figs. 7(a)–(c) show the flow pattern map obtained by us. In these figures, we show the flow patterns of bubble, and intermittent and annular flow observed in each capillary tube with a diameter of 1.0 mm, 2.4 mm, and 4.9 mm, which were plotted simultaneously on a map at same flow orientation in order to investigate the effect of the tube diameter on the flow patterns. The crosshatched zones on the map show the regions of bubble flow, and annular flow. Notice that there is hardly any influence because of tube diameter, on the flow pattern in the present experiments range of tube diameters of 1.0 to 4.9 mm. The solid lines in Fig. 7(a) show the boundaries of flow patterns obtained by Barnea et al. [15] for a 4 mm I.D. vertical upward flow, the solid lines in (b) by Barnea et al. [15] for a 4 mm I.D. horizontal pipe, and the broken lines in (b) by Mandhane et al. [16] for horizontal pipes and the solid line in (c) by Barnea et al. [2] for a 25.5 mm I.D. vertical downward flow.

A comparison of these figures reveals that the present data which is shown by marks in those figures agree well with the lines of Barnea et al. only for small pipe size, 4 mm I.D. The boundaries proposed by Mandhane et al. [16] were determined by using about 5900 data points for the test sections of the inner diameters of 12.7 mm pipes and larger ones. Our data and the Mandhane's lines do not agree well as a whole because their pipe diameters are larger than that of ours. An especially large difference is noticed in that the separated, and the wavy flows are not observed in horizontal capillary tubes. The data for the vertical downward flow in a capillary tube was not available when we obtained our data, so we compared our data with the results taken for 25.5 mm I.D. pipe by Barnea et al. [2]. The validation is very poor. The effect of tube diameter on the flow pattern, however, is smaller in our experimental range of the tube diameter, than large diameter tube data. According to our experiments, its effect becomes appreciable if the tube diameter is larger than about 6 mm. Our map is rather similar to those of the horizontal and also the vertical upward flows except that the annular flow region is wider in our case than those in the other cases. This fact signifies that the flow patterns in a capillary tube are not severely affected by the flow direction. Physically this means that the surface tension force, has a much larger effect on the flow pattern, than the gravitational force, for a gas–liquid two-phase flow in a capillary tube less than about 5 mm in diameter.

3.4. Flow pattern maps of flat channel

Fig. 8 shows the flow pattern map classified by using the weighted mean liquid lump velocity proposed by Ide et al. [17].

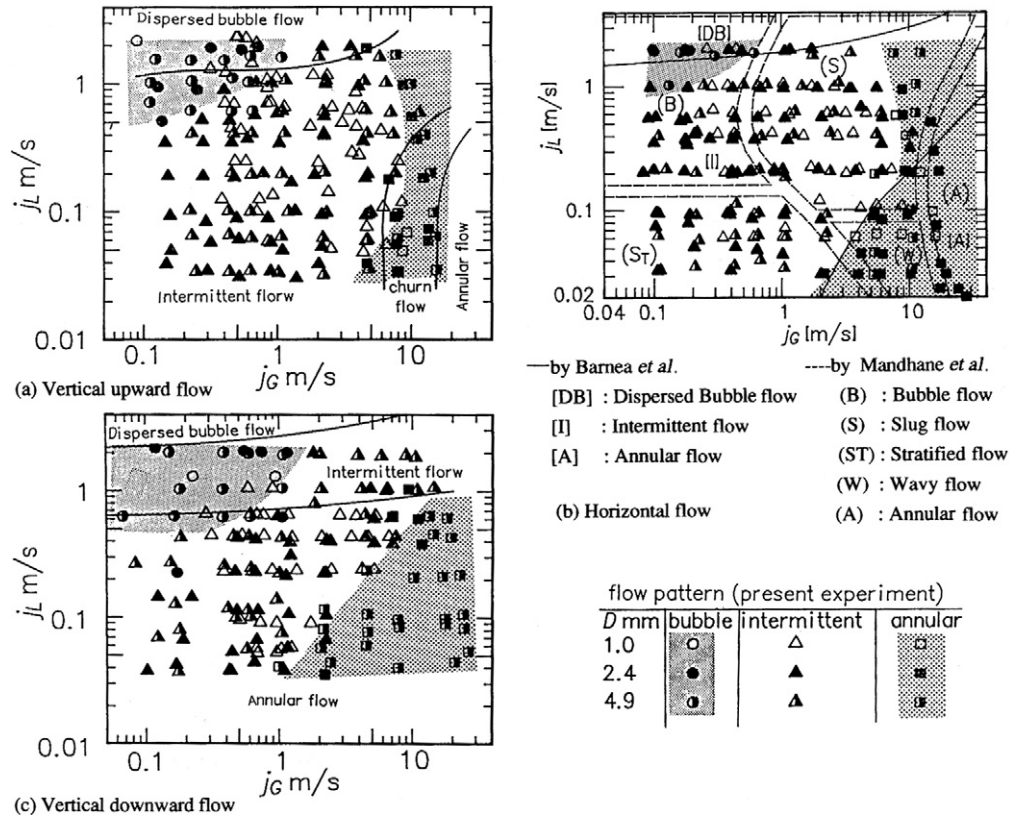

Fig. 7. Flow pattern map for circular channel.

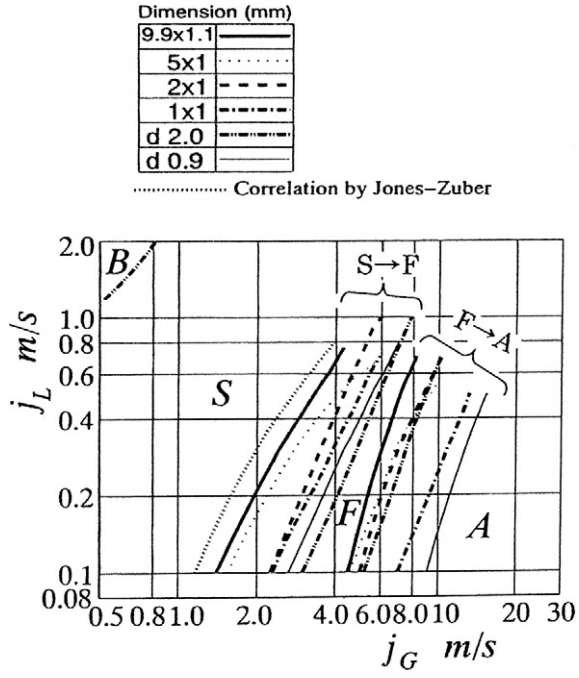

Fig. 8. Flow pattern map for flat channel.

It shows the effect by an aspect ratio of 1 to 9 of the channel cross section on the flow patterns obtained in vertical capillary flat channels. The experimental results [17] in capillary circular tubes with diameters of 2.0 mm and 0.9 mm are also shown in Fig. 8 for comparison. The symbols, S, F, and A in the figure, express the flow patterns of the slug, the froth, and the annular flow, respectively. Jones et al. [18] have proposed for the transition from the slug to the annular flow. It was, however, obtained for a channel with dimensions of 63.5 mm × 4.85 mm with a much larger equivalent diameter than that used for the present experiments. It is shown in the flow pattern map with a dotted line. It is interesting that the boundary given by Jones et al. exists relatively close to those obtained in the present experiments.

Fig. 8 shows that both the boundaries of transition from the slug flow to the froth flow regions, and from the froth flow to the annular flow regions shift to the smaller value of j_G as the aspect ratio becomes larger.

3.5. Bubble velocity in a stagnant liquid in a tube

The velocity of a large air bubble rising through a stagnant liquid in a capillary tube u_R is shown in Fig. 9 plotted against the tube diameter D. Our data is shown by solid circle and the curve as proposed by Peebles et al. [19], for bubbles in large volume, Gibson [20], for a long bubble in a vertical tube is shown for comparison. Our data corresponds well with Gibson's relation and is considerably different from the other relations. White et al. [22] also investigated the velocity in a wide range of tube diameters and fluid properties. The results are similar to those of Gibson for a small diameter tube. It should be noted that the drift velocity u_R decreases linearly with the tube diameter D and becomes zero if D becomes smaller than $D = 5.6$ mm [23]. Therefore we can consider the drift velocity

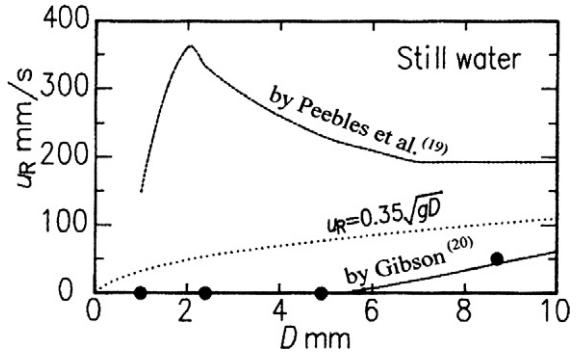

Fig. 9. Velocity of a large gas bubble rising.

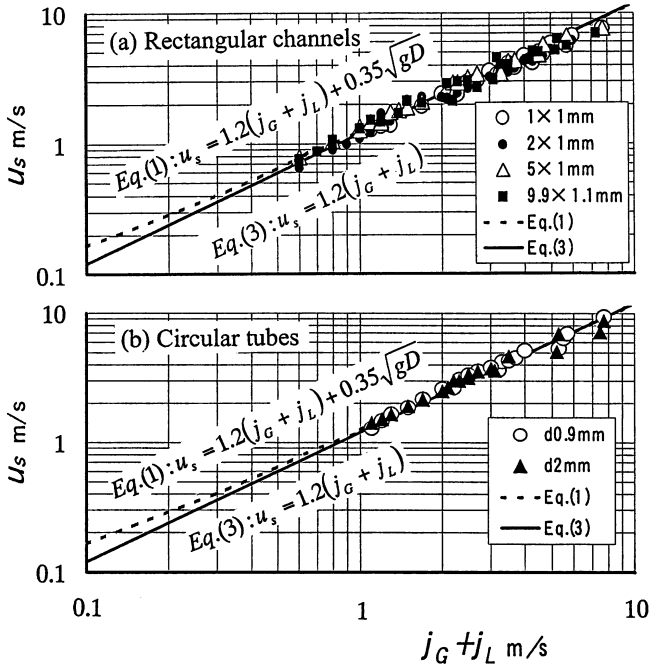

Fig. 10. Bubble velocity in two-phase flow.

due to the buoyancy force to be zero in all the capillary tubes used in the present experiment except for the 9 mm I.D. tube. Physically this shows again the strong effect of the capillary force on the shape of the nose of a large bubble, which determines the liquid rate flowing down around the large bubble as a liquid film.

3.6. Bubble velocity in two-phase flow

The bubble velocity is determined by the relation Ls/τ, where Ls is the axial distance between two electrodes measuring holdup and τ the time lag at which the cross correlation of the two holdup signals produces the maximum value.

Fig. 10 shows the bubble velocity u_s plotted against the total volumetric flux $j_T(= j_G + j_L)$ in each cases of (a) rectangular channel with the aspect ratio of 1 to 9 and (b) circular tubes with the diameter of 0.9 mm and 2.0 mm for the vertical upward flows in the minichannels. The broken line is expressed by the following correlation,

$$u_s = 1.2(j_G + j_L) + 0.35\sqrt{gD} \tag{1}$$

which was proposed by Nicklin et al. [21]. It is well known that this correlation gives an accurate estimation of u_s for a vertical upward flow in a tube of a rather large diameter, 26 mm for example, i.e., for an inertia-dominated regime. We find that the relation for vertical downward flow in the 2.4 mm I.D. tube can be given by the following equation, however, this relation is not shown in Fig. 10,

$$u_s = 1.2(j_G + j_L) - 0.35\sqrt{gD} \tag{2}$$

which is introduced by considering the second term on the right-hand side of Eq. (1) which expresses the relative velocity u_R due to the buoyancy force.

As clearly seen from Fig. 10 both Eqs. (1) and (2) do not give accurate estimations in capillary tubes irrespective of the flow direction in the low flow rate range. The Nicklin's equation is not useful when u_R is effectively zero and j_T is rather small. Following relation gives rather good estimations,

$$u_s = (1 + C_s)(j_G + j_L) \tag{3}$$

where C_s is constant and is approximately equal to 0.2 for the thick solid lines shown in Fig. 10. This fact corresponds quite well with one of the fundamental characteristics of the capillary tube flow, i.e., the nearly zero drift velocity in the case where the tube diameter is less than about 5 mm as discussed in the previous section.

Physically this means that a liquid slug moves as if it is a solid body with the velocity equal to a large air bubble. On the other hand, in the case of a vertical upward flow in a larger diameter tube, C_s takes about 0.2 signifying the existing of the non-zero drift velocity. Furthermore C_s takes about 0.2 and decreases with $(j_G + j_L)$ upward to about zero even in a horizontal line. This means the large air bubble can move faster than the liquid because it flows in the center part of the channel where the velocity is higher and the liquid is deflected toward the bottom of the tube.

If the total volumetric flux $(j_G + j_L)$ is large, the term $0.35\sqrt{gD}$ is negligibly small, if it even exists, compared to $(j_G + j_L)$ and Eq. (3) gives a good estimation of u_s as shown in Fig. 10. With a further increase in $(j_G + j_L)$, u_s decreases rather abruptly. This means the flow pattern changed from the slug flow or intermittent flow to the annular flow.

3.7. Frictional pressure drop

Fig. 11 shows the ratio of error for the estimation of two-phase friction multiplier $\Phi_L - \Phi_{LCH}$ to Φ_{LCH}. The multiplier was presented experimentally by Lockhart and Martinelli [24] and its correlation was proposed by Chisholm and Laird [25] and by Chisholm [26] as follows,

$$\phi_{LCH} = \sqrt{1 + C/\chi + (1/\chi)^2} \tag{4}$$

The parameter χ is the Martinelli parameter [24]. The errors are quite large in the range of $\chi = 1$–10 in the case of the horizontal capillary tubes while it is small in the case of large diameter tube. The flow conditions where the error becomes

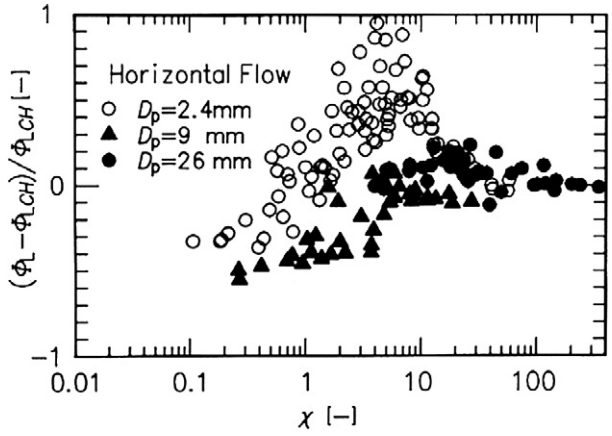

Fig. 11. Error of the estimation of two-phase multiplier.

large roughly correspond to those of the intermittent flow region. Under these condition of flow Φ_L is expressed as follows (Fukano et al. [4]);

$$\phi_L^2 = k\frac{\rho_T}{\rho_L}\left(\frac{\upsilon_T}{\upsilon_L}\right)\left(\frac{j_G + j_L}{j_L}\right)^{n+1} Re_L^{n-m} \tag{5}$$

Where the suffix 'L' means the liquid single flow, 'T' the two-phase flow, and we assumed the pressure loss occurs in the liquid slug only. This means that the static pressure is uniform in a large gas bubble. If we recognize that small bubbles rarely exist in a liquid slug as discussed in the previous section, we can adequately assume that the liquid flow in a liquid slug is similar to that of a single liquid flow. And accordingly if we consider both the single and the two-phase liquid flows are laminar, for example, then $n = m = -1$ in Eq. (5).

$$\phi_L^2 \cong 1 \tag{6}$$

On the contrary experimental values of Φ_L^2 were found to be much larger than one in the flow conditions satisfying the assumption [4] that the both flows are laminar. This discrepancy suggests that there is some mechanism to cause pressure loss other than wall friction.

We propose the mechanism of large increase in the pressure loss in the intermittent region as shown in Fig. 11 as follows. To save time we consider the following simple process. As shown in Fig. 12(a) a large gas bubble starts moving up from the closed bottom of a vertical mini tube, and comes out of the top end of the tube as shown in Fig. 12(c) through a example shown in Fig. 12(b). What happened in this short and simple process? It is clear that the liquid column above the large gas bubble in Fig. 12(a) flows down to the bottom of the tube, which signifies that the liquid column loses potential energy during this process due to the relative velocity between the large gas bubble and liquid column which is equivalent to a liquid slug. The lost potential energy at first transferred to kinetic energy of a liquid film flowing down around the large bubble and dissipating in the wake of the large bubble by mixing the liquid in the wake with the liquid rushing into there with high kinetic energy.

Even in a horizontal flow a non-zero relative velocity usually exists in a mini tube because the large bubbles flow in the center, i.e., the higher velocity region in the cross section of the tube.

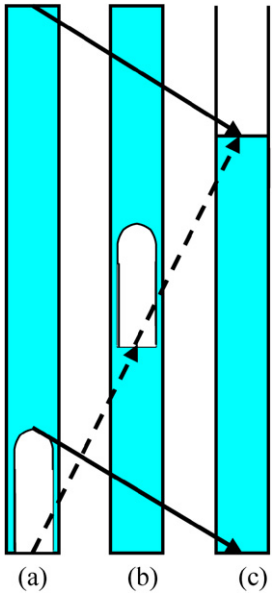

Fig. 12. Example of a large gas bubble ascending in a liquid column.

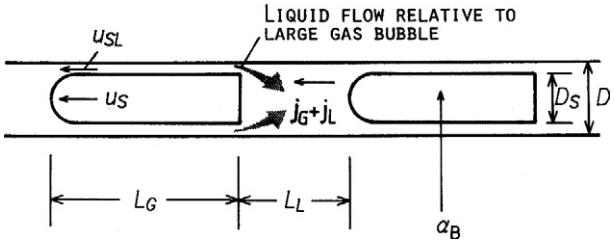

Fig. 13. Flow model.

And accordingly similar energy mixing loss is caused in the wake of the large bubble. This is the reason, that the energy loss, in the gas–liquid two-phase flow, is larger than a single phase flow especially in the intermittent flow region.

We then introduced the following plug flow model to explain the energy loss as shown in Fig. 13. That is, we consider that the pressure loss is caused mostly by two mechanisms; one is the ordinary friction loss, ΔP_f. The other one is caused by the so-called sudden expansion of liquid flow, from a liquid film surrounding a long air bubble, to a liquid slug following the long air bubble. Then,

$$P_T = \Delta P_f + \Delta P_e \tag{7}$$

Based on our experimental results we assume that (1) the void fraction in the liquid slug is zero, and (2) the liquid film is distributed uniformly around the circumference of the air bubble. Under these assumptions ΔP_f and ΔP_e are given by Eqs. (8) and (9), respectively [4]. ΔP_e is strongly affected by the void fraction in the cross section of a large gas bubble as follows.

$$\Delta P_f = \lambda\frac{L}{D}\frac{\rho_T(j_G + j_L)^2 L_L}{(L_G + L_L)} \tag{8}$$

$$\Delta P_e = \rho_L\frac{w^2 L}{2(L_G + L_L)} \tag{9}$$

$$w = \frac{(j_G + j_L) - [j_L - (j_G + j_L)(1-\gamma)]}{\gamma(1-\alpha_B)} \tag{10}$$

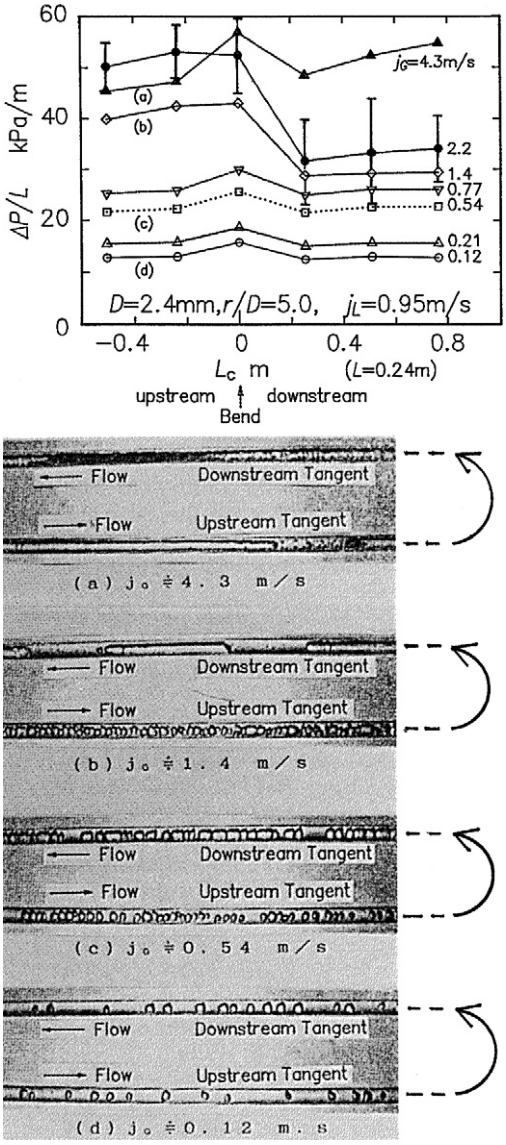

Fig. 14. Distribution of the flow pattern and pressure gradient along pipe axis through a bend.

$$\gamma = L_G/(L_G + L_L) \tag{11}$$

The calculated values of the ratio of ΔP_e to ΔP_f show that ΔP_e becomes much larger than ΔP_f in some flow conditions, especially when the number of air bubbles, or equivalently, that of the sudden expansion included in a unit length is large, which means it is one of the important factors to control the magnitude of ΔP_e. The pressure loss ΔP_e is inevitable also in a vertical flow.

The importance of ΔP_e in a horizontal line is corroborated by the following experimental results. Figs. 14(a)–(d) show the change of flow patterns caused during two-phase mixture passing through a return bend placed in a horizontal plane [5]. In the case of Fig. 14(b) the flow pattern changes drastically from a short air-bubble-chain flow to a fully developed plug flow. As shown in the figure above, the pressure gradient drastically changed in accordance with the drastic change of flow pattern. The vertical short bars attached to the data of $j_G = 2.2\ \mathrm{m\,s^{-1}}$, for example, show the standard deviation of the time varying pressure which are not caused by accidental errors but caused by the fluctuating nature of two-phase flow.

Based on this flow model we propose a correlation of frictional pressure loss. It will be discussed in the next section.

3.8. Correlation of frictional pressure drop

The values of C in Eq. (4) were experimentally investigated by Wambsganss et al. [9], Kawaji et al. [10] and Mishima et al. [27] for rectangular channels. Kawaji et al. pointed out that the depth of a channel or the clearance and j_L affect the value of C. Wambsganss et al. showed that C increases from 5 to 20 with increasing j_L. According to the examination of the present experimental results of j_L there is a tendency for C to approach 21 with increase in both j_L and χ, and to approach 5 when j_L and χ are small. We noticed that the effect of j_L on Φ_L is large as is also seen in the results obtained by Wambsganss et al. and Kawaji et al.

Furthermore we examined the applicability of the Lockhart–Martinelli (L-M) correlation to the two-phase flow in minichannels and we concluded that the original L-M correlation is not useful in predicting two-phase frictional pressure drop in minichannels. Accordingly, we examined the applicability of the revised L-M correlations also, which have been proposed by Mishima et al. [27], Wambsganss et al. [9] and Friedel et al. [28]. As a result we found that satisfactory correlations have not been obtained in any of our cases because the effects of mass velocity of liquid, i.e. j_L are not fully taken into account in their correlations.

In our research, the value of C in Eq. (4) is obtained following the method proposed by Wambsganss et al. as follows:

$$C = 0.15 Re_L^{0.61} \tag{12}$$

Even if Eq. (12) is used a fundamental improvement is not obtained. These discussions lead to the conclusion that we need a different type of correlation.

3.9. Correlations by the produced authors

In order to predict the two-phase pressure drop in horizontal capillary circular tubes we produced Eq. (13) based on the flow model discussed in Fig. 13. In introducing Eq. (13), we discriminated on the flow patterns of the intermittent flow (slug and froth flows) from annular flow in a capillary tube by the simple method shown as follows.

First of all we characterized the laminar flow (V) or the turbulent flow (T) of a two-phase intermittent flow in a capillary circular tube by using the liquid Reynolds numbers in water single-phase flow and two-phase flow, where j_L and $(j_G + j_L)$ are taken as the characteristic velocities, respectively. For example, when a water single phase flow is laminar (V) and a two-phase flow is turbulent (T), the flow is referred to as VT. Then, the critical Reynolds number from laminar flow to turbulent flow is taken as 2400.

For the VT region in a capillary circular tube,

$$\phi_L = 0.0837\left\{(j_G + j_L)/j_L\right\}^{0.425} Re_L^{3/8} \tag{13}$$

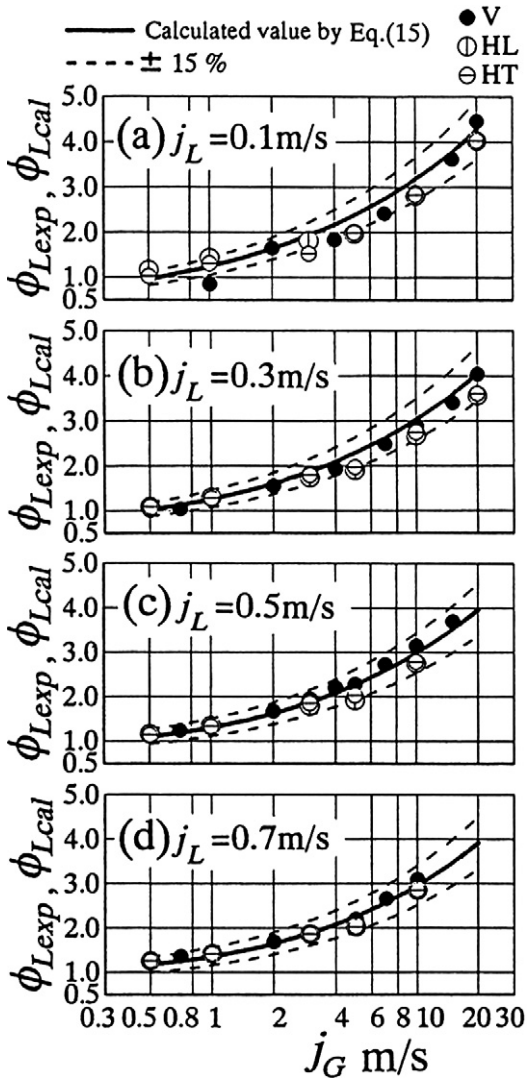

Fig. 15. Comparison of experimental results of ϕ_L with the calculation of Eq. (15).

In the same way a correlation for vertical capillary flat channels with the aspect ratio T_S of 1 to 9 is expressed as follows.

For the VV region in a capillary rectangular channel,

$$\phi_L = 0.2485 T_S^{-0.355} \left\{ j_L / \sqrt{g D_h} \right\}^{-0.233} Re_L^{3/8} \tag{14}$$

For the VT region in a capillary rectangular channel,

$$\phi_L = 0.0848 T_S^{-0.145} \left\{ (j_G + j_L)/j_L \right\}^{0.425} Re_L^{3/8} \tag{15}$$

where Re_L is the same liquid Reynolds number as defined previously.

In the experimental results obtained in a flat channel with the aspect ratio of 9, Eq. (15) only was used, since there was little data included in the VV region.

Fig. 15 shows the comparison of our experimental results $\phi_{L\,exp}$ of the two-phase frictional pressure drop obtained in a channel of 9.9 mm × 1.1 mm with the calculated values ϕ_{Lcal} by Eq. (15). We have validated that the two-phase frictional pressure drop in horizontal and vertical capillary rectangular channels can be estimated by Eq. (15) with sufficient accuracy.

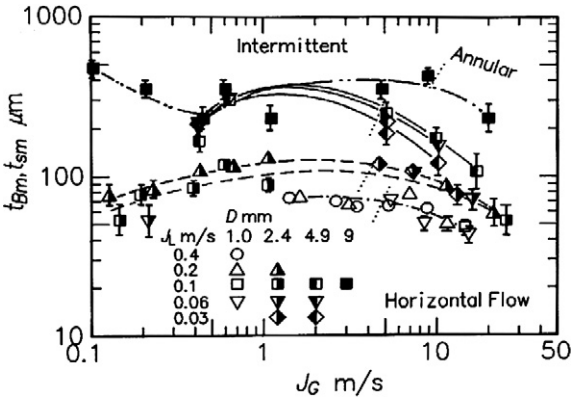

Fig. 16. Liquid film thickness.

3.10. Film thickness

Fig. 16 shows the film thickness around long gas bubbles averaged over their full lengths in the horizontal tube. The base film thickness in annular flow is also plotted against the air superficial velocity, with the liquid superficial velocity, and the tube diameter being the parameters. In addition the film thickness in a 9 mm I.D. tube determined by assuming the circumferential distribution of film thickness is uniform, although this assumption is not as described before, is also plotted for comparison. The error in measuring film thickness was 6%–2% in 1 mm I.D. pipe, 19%–9% in 2.4 mm I.D. pipe, 24%–6% in 4.9 mm I.D. pipe and 17%–8% in 9 mm I.D. pipe. As clearly shown in Fig. 16 the film thickness decreases by decreasing the tube diameter, because, the pressure difference between the outside and the inside of the air bubble becomes larger, i.e. the bubble becomes more rigid, as the tube diameter becomes smaller due to the surface tension force, and accordingly it becomes more difficult for liquid to pass by the long bubble. For the same reason, the film thickness decreases, with the decrease in superficial air velocity j_G, in the case of the capillary tube, i.e., $D = 1$, 2.4 and 4.9 mm. On the other hand, in the example of the rather large diameter, 9 mm I.D., tube the film thickness increases with decreasing j_G. The lower the air velocity, the larger the difference in film thickness. We also noticed that the film thickness around the long bubble in intermittent flow, i.e., slug and froth flow, can be easily correlated to the base film thickness, in annular flow, as the air flow rate increases.

3.11. Mean holdup

Figs. 17(a)–(d) show the change in the mean holdup η_{mean} plotted against j_G in which the effects of the aspect ratio of the test section on η_{mean} are clarified. The data is plotted for five different values of j_L, ranging from 0.1 m s^{-1} to 0.7 m s^{-1}. Each of the five lines on each figure corresponds to the mean holdup of the respective liquid flow condition, which is calculated with the following equation previously proposed by us for a vertical capillary channel.

$$\eta_{mean\,CAL} = 1 - \left[1 + 1.86 \times 10^3 E\ddot{o}^{0.75} Fr^{0.95} \times Re^{-1.03} Ca^{0.17} (j_L/j_G) \right]^{-1} \tag{16}$$

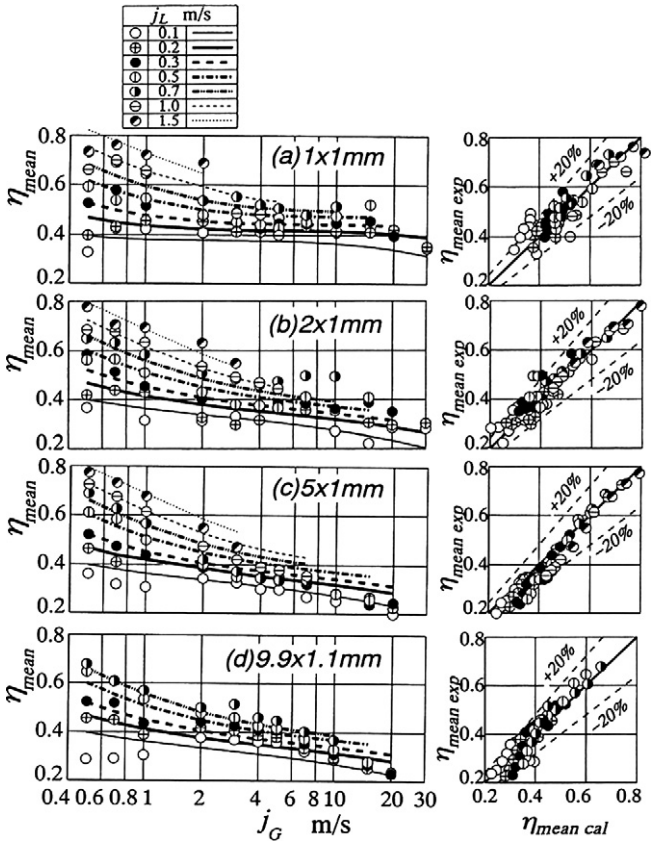

Fig. 17. Time averaged mean holdup.

where $E\ddot{o}$ is the Eötvös number $\{\equiv (\rho_L - \rho_G) g D_e^2/\sigma_L\}$ using the characteristic length, D_e defined by Sadatomi et al. [29]. Fr is the Froude number $\{\equiv (j_G + j_L)/\sqrt{gD_e}$, Re the Reynolds number$(\equiv G D_e/\mu_m)$, and Ca the Capillary number $\{\equiv \mu_m(j_G + j_L)/\sigma_L\}$. The parameter G used in Re is the total mass velocity, $G = G_G + G_L = \rho_G j_G + \rho_L j_L$ and σ_L is the surface tension of the liquid and μ_m the two-phase viscosity. In this paper, the two-phase viscosity is expressed by the following correlation, Eqs. (17).

For the channels of $E\ddot{o} \geqslant 0.3$,

$$\mu_m = 0.57\mu_L\big[\beta/(1-\beta)\big]^{-0.15} = 0.57\mu_L(j_G/j_L)^{-0.15} \quad (17.1)$$

For the channels of $E\ddot{o} < 0.3$ (for a channel of 1.0 mm × 1.0 mm), the following equation produces a better accuracy.

$$\mu_m = 0.45\mu_L\big(j_G/j_L\big)^{-0.15}\big\{(j_G + j_L)/\sqrt{gD_e}\big\}^{0.13} \quad (17.2)$$

where $\beta\{\equiv j_G/(j_G + j_L)\}$ is the ratio of the gas to the mixture volume flow rates.

From Fig. 17 we can see the effect of j_L on the mean holdup and we point out that when the aspect ratio becomes large, η_{mean} in the region of large j_G tends to decrease with increasing of j_G and in contrast to it, η_{mean} in the small aspect ratio, in particular, in the channel of 1.0 mm × 1.0 mm does not change much over the relatively wide range of j_G and η_{mean} is large in the region of froth flow and annular flow.

The reason that η_{mean} increases in a small aspect ratio is considered to be that the liquid is held at the corners of the cross section of the channel by the effects of surface tension and viscosity. This effect seems to lead to an increase in the velocity of the gas flow in the central portion of the channel and to raise slip ratio in a capillary channel.

4. Conclusions

We experimentally examined the characteristics of an air–water isothermal two-phase flow in capillary tubes with the inner diameter of 1 mm, 2.4 mm, 4.9 mm as well as in capillary rectangular channels with the aspect ratio of 1 to 9 while using the data in 9 mm and 26 mm circular tubes as the comparison with the ducts with a large cross section. The directions of flow were vertical upward, horizontal and vertical downward. We also proposed correlations of the holdup and the frictional pressure drop. The results are summarized as follows:

(A) Common to the both minichannels:
  (1) Capillary force becomes important in the case that the equivalent diameter is less than 5 mm.
  (2) Flow pattern does not change much according to the flow direction.

(B) For the circular tube:
  (3) Separated flow was not observed in any flow conditions tested in the present experiments.
  (4) Even in the horizontal flow the flow pattern becomes axisymmetrical, and the water film thickness is circumferentially uniform.
  (5) Small bubbles usually do not exist in liquid slugs and liquid films.
  (6) Drift velocity is approximately zero independent of the flow direction. And the bubble velocity approaches to the total volumetric flux j_T as j_T becomes small.
  (7) The frictional multiplier becomes very large compared to the predictions by the Chisholm's correlation in the intermittent flow. In that case the pressure loss caused at the tail of long bubble due to the sudden expansion of flow field of liquid flow becomes important.

(C) For the mini flat channel:
  (8) The effects of the aspect ratio on the flow pattern map, the mean holdup and the two-phase frictional pressure drop were made clear in vertical channels.
  (9) The differences between the vertical and the horizontal channel cause noticeable differences in the measured parameters in the annular flow region where j_G is larger than about 10 m s^{-1}. That is, the mean holdup is smaller in the vertical channel than in the horizontal channel. On the other hand, the two-phase frictional pressure drop and the passing frequency of the liquid lumps are larger in the vertical channel than in the horizontal channel.
  (10) In the horizontal channel, the effects of the difference in the channel setting, longitudinal or transverse, are small on the measured parameters.

(11) We proposed the correlations for the mean holdup and for the two-phase frictional pressure drop. The predictions obtained from these correlations have sufficient accuracy for both the vertical and the horizontal cases.

References

[1] M. Suo, P. Griffith, Two-phase flow in capillary tubes, ASME J. Basic Eng. (1964) 576–582.

[2] D. Barnea, O. Shoham, Y. Taitel, Flow pattern transition for vertical downward two phase flow, Chem. Eng. Sci. 37 (5) (1982) 741–744.

[3] C.A. Damianides, J.W. Westwater, Two-phase flow patterns in a compact heat exchanger and in small tubes, in: Proceedings of the Second UK National Conf. On Heat Transfer, Glasgow, 14–16 September, Mechanical Engineering Publications, London, 1988, pp. 1257–1268.

[4] T. Fukano, A. Kariyasaki, M. Kagawa, Flow patterns and pressure drop in isothermal gas–liquid concurrent flow in a horizontal capillary tube, Trans. JSME B 56 (528) (1990) 2318–2326.

[5] A. Kariyasaki, T. Fukano, A. Ousaka, M. Kagawa, Characteristics of time-varying void fraction in isothermal air–water concurrent flow in a horizontal capillary tube, Trans. JSME B 57 (544) (1991) 4036–4043.

[6] K. Mishima, T. Hibiki, Effect of inner diameter on some characteristics of air–water two-phase flows in capillary tubes, Trans. JSME Ser. B 61 (589) (1995) 3197–3204.

[7] L. Troniewski, R. Ulbrich, Two-phase gas–liquid flow in rectangular channels, Chem. Eng. Sci. 39 (1984) 751–765.

[8] B. Lowry, M. Kawaji, Adiabatic vertical two-phase flow in narrow flow channels, AIChE Symp. Ser. 84 (263) (1988) 133–139.

[9] M.W. Wambsganss, J.A. Jendrzejczyk, D.M. France, N.T. Obot, Frictional pressure gradients in two-phase flow in a small horizontal rectangular channel, Int. J. Exp. Thermal Fluid Sci. 5 (1) (1992) 40–56.

[10] M. Ali, M. Sadatomi, M. Kawaji, Adiabatic two-phase flow in narrow channels between two flat plates, Can. J. Chem. Eng. 71 (5) (1993) 657–666.

[11] T. Wilmarth, M. Ishii, Two-phase flow regimes in narrow rectangular vertical and horizontal channels, Int. J. Heat Mass Transfer 37 (12) (1994) 1749–1758.

[12] K.A. Triplett, S.M. Ghiaasiaan, S.I. Abdel-Khalik, A. LeMouel, B.N. McCord, Gas–liquid two-phase flow in micro channels. Part II: Void fraction and pressure drop, Int. J. Multiphase Flow 25 (1999) 395–410.

[13] J.L. Xu, P. Cheng, T.S. Zhao, Gas–liquid two-phase flow regimes in rectangular channels with mini/micro gaps, Int. J. Multiphase Flow 25 (1999) 411–432.

[14] T. Fukano, Measurement of time varying thickness of liquid film flowing with high speed gas flow by a constant electric current method (CECM), Nuclear Eng. Design 184 (1998) 363–377.

[15] D. Barnea, Y. Luninski, Y. Yaitel, Flow in small diameter pipes, Can. J. Chem. Eng. 61 (1983) 617–620.

[16] J.M. Mandhane, G.A. Gregory, K. Aziz, A flow pattern map for gas–liquid flow in horizontal pipes, Int. J. Multiphase Flow 1 (1974) 537–553.

[17] H. Ide, H. Matsumura, T. Fukano, Velocity characteristics of liquid lumps and its relation to flow patterns in gas–liquid two-phase flow in vertical capillary tubes, in: Gas Liquid Flow, Book No. G00975, in: FE, vol. 19, 1995, pp. 1–8.

[18] O.C. Jones, N. Zuber, Two-Phase Momentum, Heat and Mass Transfer in Chemical, Process, and Energy Engineering System, vol. 1, McGraw-Hill, NY, 1979, pp. 345–355.

[19] F.N. Peebles, H.J. Garber, Studies on the motion of gas bubbles in liquid, Chem. Eng. Prog. 49 (2) (1953) 79–88.

[20] A.H. Gibson, On the motion of long air-bubbles in a vertical tube, Phil. Mag. 26 (156) (1913) 952–965.

[21] D.J. Nicklin, J.O. Wilke, J.F. Davidson, Two-phase flow in vertical tubes, Trans. Inst. Chem. Eng. 40 (1) (1962) 61–68.

[22] E.T. White, R.H. Beardmore, The velocity of single cylindrical air bubbles through liquids contained in vertical tubes, Chem. Eng. Sci. 17 (1962) 351–361.

[23] F.P. Bretherton, The motion of long bubbles in tubes, J. Fluid Mech. 10 (1961) 166–188.

[24] R.W. Lockhart, R.C. Martinelli, Proposed correlation of data for isothermal two-phase, two-component flow in pipes, Chem. Eng. Prog. 45 (1949) 39–48.

[25] D. Chisholm, A.D.K. Laird, Two-phase flow in rough tubes, Trans. ASME 80 (2) (1958) 276–286.

[26] D. Chisholm, A theoretical basis for the Lockhart–Martinelli correlation for two-phase flow, Int. J. Heat Mass Transfer 10 (1967) 1767–1778.

[27] K. Mishima, T. Hibiki, H. Nishihara, Some characteristics of gas–liquid flows in narrow rectangular ducts, Int. J. Multiphase Flow 19 (1993) 115–124.

[28] L. Friedel, Improved friction pressure drop correlation for horizontal and vertical two-phase pipe flow, in: European Two-Phase Flow Group Meeting, Ispra, Italy, Paper E2, 1979.

[29] M. Sadatomi, Y. Sato, S. Saruwatari, Two-phase flow in vertical noncircular channels, Int. J. Multiphase Flow 8 (6) (1982) 641–655.